minerals

MDPI

Article

Stability of $AuCl_2^-$ from 25 to 1000 °C at Pressures to 5000 bar and Consequences for Hydrothermal Gold Mobilization

Alexander V. Zotov, Nikolai N. Kuzmin, Vladimir L. Reukov and Boris R. Tagirov *

Institute of Geology of Ore Deposits, Petrography, Mineralogy and Geochemistry (IGEM RAS), 35 Staromonetnyi per., 119017 Moscow, Russia; avzotov36@mail.ru (A.V.Z.); kolyanfclm@gmail.com (N.N.K.); azotov@igem.ru (V.L.R.)

* Correspondence: boris1t@yandex.ru

Received: 10 May 2018; Accepted: 2 July 2018; Published: 4 July 2018

Abstract: Gold is transported in high-temperature chloride-bearing hydrothermal fluids in the form of $AuCl_2^-$. The stability of this complex has been extensively studied, but there is still considerable disagreement between available experimental data on the temperature region 300–500 °C. To solve this problem, we measured the solubility of gold in HCl/NaCl fluids (NaCl concentration varied from 0.1 to 3 mol·(kg·H_2O)$^{-1}$) at 450 °C and pressures from 500 to 1500 bar (1 bar = 10^5 Pa). The experiments were performed using a batch autoclave method at contrasting redox conditions: in reduced experiments hydrogen was added to the autoclave, and in oxidized experiments the redox state was controlled by the aqueous SO_2/SO_3 buffer. Hydrogen pressure in the autoclaves was measured after the experiments in the reduced system. The gold solubility constant, $Au_{(cr)} + HCl^\circ_{(aq)} + Cl^- = AuCl_2^- + 0.5\ H_2{}^\circ_{(aq)}$, was determined for the experimental *T*-*P* parameters as $\log K_s^\circ = -4.77 \pm 0.07$ (500 bar), -5.11 ± 0.08 (1000 bar), and -5.43 ± 0.09 (1500 bar). These data, together with values from the literature for temperatures from 25 to 1000 °C, were fitted to the simple equation $\log K_s^\circ = 4.302 - 7304 \cdot T(\mathrm{K})^{-1} - 4.77 \cdot \log d(\mathrm{w}) + 11080 \cdot (\log d(\mathrm{w})) \cdot T(\mathrm{K})^{-1} - 6.94 \times 10^6 \cdot (\log d(\mathrm{w})) T(\mathrm{K})^{-2}$, where d(w) is the pure water density. This equation can be used together with the extended Debye–Hückel equation for activity coefficients to calculate gold solubility at pressures up to 5000 bar at fluid chlorinities at least up to 30 wt %. The speciation of gold in natural chloride-bearing fluids is discussed.

Keywords: gold; solubility; hydrothermal solutions; chloride complex; experiment; thermodynamic modeling

1. Introduction

Chlorine is the most important component of natural fluids. Fluid chlorinity, together with acidity and redox state, controls the concentration of many ore metals, which can migrate in the fluid phase in the form of chloride complexes. The chlorinity of natural ore-forming fluids varies in a wide range. For example, solutions migrating in seafloor hydrothermal systems at temperatures from 250 to 400 °C are relatively diluted (~3 wt % NaCl eq., Seward et al. [1]), whereas the magmatic brines of porphyry systems may contain up to 50–60 wt % NaCl eq. at ~750 °C (Ulrich et al. [2]). In these fluids Au can be efficiently transported in the form of the Au(I)-Cl complexes [1]. The complexation of Au in chloride solutions has been extensively studied by potentiometry, solubility experiments, X-ray absorption spectroscopy, and ab initio molecular dynamics (AIMD). Nikolaeva et al. [3] determined the potential of Au electrode in 1 M (mol·L^{-1}) NaCl + Au(I) solution at 25–80 °C. The authors attributed the measured potentials to the reaction between the Au electrode and $AuCl_2^-$. The solubility of

Au in chloride solutions was studied by Gammons and Willams-Jones [4] at 300 °C, Zotov et al. [5] at 350–500 °C (see also references in this paper), and Stefánsson and Seward [6] at 300–600 °C. These authors [4–6] determined the formation constants of $AuCl_2^-$—the dominant Au complex in chloride-rich fluids—and calculated the thermodynamic properties of this complex. The Au solubility constants determined by Zotov et al. [5] are ~1.5 log units higher than those reported by Stefánsson and Seward [6] for similar *T-P* parameters. Au–Cl complexation at higher temperatures (750–1000 °C) was studied by Ryabchikov and Orlova [7], Zajacz et al. [8], and Guo et al. [9]. The dominant role of $AuCl_2^-$ in chloride-rich fluids was confirmed by X-ray absorption spectroscopic experiments performed at 250 °C (Pokrovski et al. [10]). Mei et al. [11] interpreted the results of AIMD simulations in terms of the formation of the $NaAuCl_2^\circ$ ion associate, which was found to predominate over $AuCl_2^-$ at fluid densities $d < 0.7$ g·cm^{-3}. The solubility of Au in low-density vapor was determined by Archibald et al. [12].

The aim of our study is to obtain new experimental data on Au solubility, determine the stability of the dominant Au–Cl complex at an intermediate temperature of 450 °C, and resolve the disagreement between the key studies of Au–Cl complexation [5,6]. The uncertainty of redox potential is an important source of errors in the Au solubility constant. To eliminate this error, we performed solubility experiments under contrasting redox conditions: reduced (with the addition of hydrogen to the experimental system) and oxidized (with the sulfite (SO_2)/sulfate (SO_3) redox buffer). After all experiments under reduced conditions, hydrogen pressure was measured in the experimental system. Combining the two sets of data obtained in the reduced and oxidized systems, we obtained reliable values for the stability constant of the dominant Au complex, $AuCl_2^-$, free of error related to redox potential uncertainty. These new values were pooled with the literature data and fitted to a simple density model equation. The resulting equation enables accurate estimation of Au solubility in chloride fluids in a wide range of fluid chlorinity and over the whole range of *T-P* parameters characteristic of hydrothermal systems, up to temperatures of 1000 °C and pressures of 5000 bar. Based on this new model, the speciation and concentration of Au in natural chloride-bearing fluids are discussed.

2. Materials and Methods

2.1. Experimental

Solubility experiments were performed using two methods of redox control. To impose reduced conditions, hydrogen was added into the autoclave, and its pressure was measured after the experiment. The redox state of the oxidized system was controlled by the SO_2/SO_3 buffer.

2.1.1. Reduced Conditions

The solubility measurements were performed at 450 °C and pressures of 500 and 1000 bar using Ti autoclaves (VT-8 alloy) with a volume of 20 cm^3. A needle valve allowing gas pressure measurement was built in the cup of the autoclave (Kudrin [13]). Prior to the experiments the autoclaves were passivated with an HNO_3-H_2O (1:3 by volume) mixture at 400 °C and 500 bar. The total pressure in the autoclave was controlled by the degree of filling using the *PVT* properties of the H_2O-NaCl system (Driesner [14]; Driesner and Heinrich [15]). The uncertainty of total pressure was estimated as ±2%. Experimental solutions were prepared from distilled water, extra pure NaCl, and 0.1 M HCl fixanal. A piece of Au net (99.99%) with an outer surface of 1.5–3 cm^3 was fixed in the upper part of the autoclave. The autoclave was loaded in air. A weighed Al chip (99.9%) was used to produce hydrogen upon heating via the reaction: $Al + 2H_2O \rightarrow AlOOH + 1.5\ H_{2(g)}$. The loaded autoclave was hermetically closed and placed in a gradient-free furnace. During the experiment, temperature was controlled within ±2 °C using a K-type thermocouple. The duration of the experiments varied from 5 to 12 days, which was sufficient for equilibration (Zotov and Baranova [16]). After the experiment, the autoclave was quenched in cold water. The hydrogen pressure in the autoclave was measured after quenching: the internal valve inside the autoclave cap was opened and hydrogen from the

autoclave passed into an external cell with a built-in pressure piezometer. The volume of the cell was 6.7 cm^3. The piezometer was calibrated at atmospheric pressure and in vacuum (5×10^{-5} bar); its readings before the measurements were verified against an external reference pressure gauge in the pressure range 2–5 bar. The measured value was corrected for the pressure of atmospheric nitrogen (0.8 bar). We estimated the uncertainty of hydrogen pressure determination as ±10%. This uncertainty is accounted for mostly by the presence of nitrogen. After hydrogen pressure measurement, the autoclave was opened and the quench solution was extracted and diluted with an equal volume of aqua regia. Then the autoclave was filled with hot aqua regia and kept for 30 min at 70–80 °C, after which the washing solution was diluted with an equal volume of distilled H_2O. Finally the solution was diluted with 6 M HCl to match the concentration range suitable for analysis. The concentration of dissolved Au was analyzed by inductively coupled plasma mass spectrometry (ICP-MS) on an X Series 2 Thermo Scientific mass spectrometer, Waltham, MA, USA. The accuracy of the analysis was ±5% at the 95% confidence level, and the detection limit was 0.1 ppb. It was found that a considerable amount of dissolved Au (20–50%) was deposited on the autoclave walls during quenching.

The concentration of hydrogen in the experimental fluids calculated from the measured hydrogen pressure was lower than the initial value. The hydrogen loss varied from 20% to 90% at 500 bar and from 40% to 99% at 1000 bar. Hydrogen escaped through the needle valve and the autoclave seal. The hydrogen loss was not reproducible and, usually, increased after several experiments owing to the seal ring wear. The concentration of dissolved Au increased during the experiment. We believe that the kinetics of Au dissolution is fast enough to attain equilibrium Au concentration at any hydrogen pressure. This assumption is confirmed by the excellent agreement between Au solubility constants obtained from the Au solubility data under reduced and oxidized conditions (see next section). Therefore, the Au concentrations of experimental solutions determined after the experiments are considered identical to the equilibrium Au solubilities for given *T*-*P*-*f*(H_2) parameters.

2.1.2. Oxidized Conditions

In the oxidized system, Au solubility was measured at 450 °C and pressures of 1000 and 1500 bar. Conventional batch Ti autoclaves (VT-8 alloy) with an internal volume of 20 cm^3 were used. The stock solutions were prepared from extra pure concentrated SO_2, H_2SO_4, HCl, and extra pure NaCl. The concentration of SO_2 was determined by iodometric titration; H_2SO_4, by densimetry; and HCl, by volumetric titration against Trizma® base (Sigma-Aldrich, St. Louis, MO, USA) with methyl red as an indicator. The procedures of autoclave loading, quenching, and solution preparation were the same as described for the reduced system. The duration of the experiments varied from 12 to 20 days.

2.2. Thermodynamic Calculations

The standard state of a pure solid phase and H_2O corresponds to a unit activity of the pure phase at a given temperature and pressure. The standard state adopted for the aqueous species is unit activity for a hypothetical one molal (m, mol·(kg·H_2O)$^{-1}$) ideal solution. The activity coefficients of charged aqueous species were calculated using the extended Debye–Hückel equation

$$\log \gamma_i = -\frac{A z_i^2 \sqrt{I}}{1 + B\overset{\circ}{a}\sqrt{I}} + \Gamma_\gamma \quad (1)$$

where the ion size parameter $\overset{\circ}{a}$ was taken to be 4.5 Å for all species, A and B are the Debye–Hückel activity coefficient parameters, I is the ionic strength, z_i is the charge of the species, and Γ_γ is the conversion factor from mole fraction to molality. For neutral species, it was assumed that $\log \gamma_n = \Gamma_\gamma = -\log (1 + 0.018 \cdot m^*)$, where m^* is the sum of the concentrations of all solute species. Speciation calculations were performed by means of the Gibbs computer code of the HCh software package (Shvarov [17]). The thermodynamic properties of the aqueous species Na^+,

Cl^-, HSO_4^-, SO_4^{2-}, HSO_3^-, SO_3^{2-}, $S_2O_3^{2-}$, K^+, $KCl^\circ_{(aq)}$ were taken from the SUPCRT92 database (Johnson et al. [18]). The thermodynamic properties of H_2O, HCl°, $NaCl^\circ$, and OH^- were adopted from Wagner and Prusss [19], Tagirov et al. [20], Ho et al. [21], and Bandura and Lvov [22], respectively; those of $H_2{}^\circ_{(aq)}$, $O_2{}^\circ_{(aq)}$, and $SO_2{}^\circ_{(aq)}$, from Akinfiev and Diamond [23]. The values of Henry constants and dissociation constants of aqueous electrolytes calculated using the aforementioned thermodynamic data are presented in the Supplementary Material Section 1. The thermodynamic properties of $Au_{(cr)}$, hematite Fe_2O_3, magnetite Fe_3O_4, $Ni_{(cr)}$, and bunsenite NiO were taken from the SUPCRT92 database [18], and those of manganosite MnO and hausmannite Mn_3O_4, from Robie and Hemingway [24]. Thermodynamic data for quartz, muscovite, K-feldspar, and andalusite were adopted from Berman [25] with corrections of Sverjensky et al. [26].

The OptimA program of the HCh package (Shvarov [27]) was used to calculate the Gibbs free energies of Au aqueous complexes. The program computes the Gibbs free energies of aqueous complexes by the least squares minimization of the difference between the calculated and experimental values of activity or total solute concentration (i.e., $m(Au_{total})$ in this study). Finally, the optimized values of the Gibbs free energies of Au complexes were recalculated, together with the corresponding confidence intervals, to the logarithms of reaction constants as $\log K = -\Delta_r G/(2.303 \cdot RT)$.

3. Results

3.1. Experimental Au Solubility Determination

The results of experiments are given in Table 1. Figure 1a,b and Figure 2a–c show that the slopes of the solubility curves vs. $\log m(H_2{}^\circ_{(aq)})$ and $\log m(Cl^-)$ are consistent, over the whole range of experimental temperature, pressure, and system composition, with the formation of $AuCl_2^-$ complex via the reaction

$$Au_{(cr)} + HCl^\circ_{(aq)} + Cl^- = AuCl_2^- + 0.5\ H_2{}^\circ_{(aq)} \quad (2)$$

for which

$$\log K_s^\circ = \log m(AuCl_2^-) + 0.5 \log m(H_2{}^\circ_{(aq)}) - \log m(Cl^-) - \log m(HCl^\circ_{(aq)}) \quad (3)$$

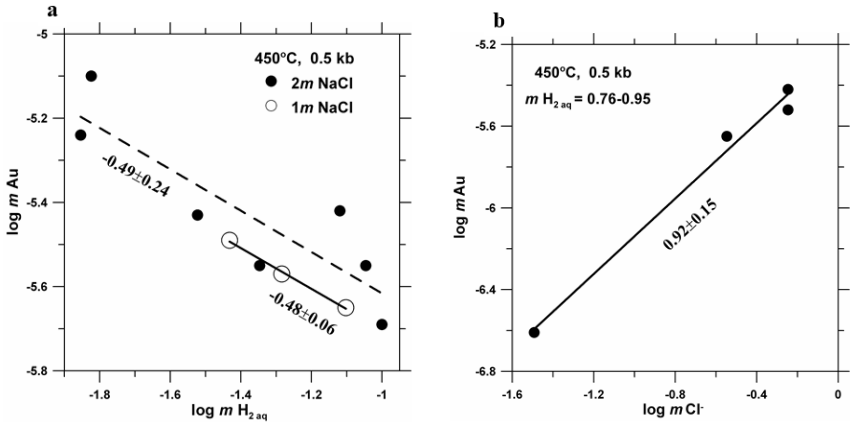

Figure 1. The concentration of Au (**a**) as a function of $H_2{}^\circ_{(aq)}$ concentration at constant fluid salinities, and (**b**) as a function of Cl^- concentration at constant dissolved hydrogen concentration. The slopes of the solubility curves are indicated in the diagrams. Experiments were performed with hydrogen added to the system (reduced conditions).

It follows from Equations (2) and (3) that the dissolved Au concentration decreases as a square root of hydrogen fugacity (at constant fluid acidity and chlorinity). The dependence of the logarithm of dissolved Au concentration on the logarithm of hydrogen molality has a slope of −0.5 (Figures 1a and 2a,b). Note that the Au solubilities determined in the systems with contrasting redox states are in

excellent agreement with the stoichiometry of Equation (2) (Figure 2b). As follows from Equations (2) and (3) and is demonstrated by Figures 1b and 2c, the concentration of Au increases proportionally to the fluid chlorinity (at constant concentrations of hydrogen and hydrochloric acid).

Table 1. Compositions of experimental solutions and results of Au solubility experiments (molal concentrations are given, mol·(kg·H_2O)$^{-1}$), t = 450 °C, P from 500 to 1500 bar.

m NaCl	*m* HCl	*m* H_2SO_4	*m* SO_2	*m* $H_{2(aq)}$	log *m* Au	Δlog *m* Au **
500 bar						
2	0.1			0.014	−5.24	0.14
2	0.1			0.03	−5.43	0.17
2	0.1			0.076	−5.42	−0.05
2	0.1			0.09	−5.55	0.05
2	0.1			0.015	−5.1	−0.01
2	0.1			0.1	−5.69	0.16
2	0.1			0.045	−5.55	0.20
1	0.1			0.037	−5.49	−0.11
1	0.1			0.079	−5.65	−0.12
1	0.1			0.052	−5.57	−0.11
0.1	0.1			0.147	−6.79	−0.02
0.1	0.1			0.095	−6.64	−0.07
0.1	0.1			0.167	−6.95	0.11
1000 bar						
2	0.1			0.0026	−5.16	0.20
2	0.1			0.057	−5.7	0.08
0.5	0.1			0.078	−5.86	−0.30
0.5	0.1			0.118	−6.34	0.09
0.5	0.1			0.0085	−5.61	−0.07
0.5	0.1			0.0082	−5.6	−0.07
0.1	0.1			0.0003	−5.28	−0.21
0.206	0.119	0.0478	0.0987	5.86×10^{-7} *	−3.69	−0.13
0.508	0.119	0.0478	0.0987	1.26×10^{-6} *	−3.62	0.01
1.018	0.119	0.0478	0.0987	2.22×10^{-6} *	−3.60	0.12
2.035	0.119	0.0478	0.0987	3.78×10^{-6} *	−3.44	0.09
3.043	0.119	0.0478	0.0987	5.07×10^{-6} *	−3.21	−0.07
1500 bar						
0.218	0.119	0.0478	0.0987	8.05×10^{-7} *	−4.10	−0.001
0.497	0.119	0.0478	0.0987	1.62×10^{-6} *	−3.93	0.04
1.012	0.119	0.0478	0.0987	2.94×10^{-6} *	−3.68	−0.05
2.038	0.119	0.0478	0.0987	5.04×10^{-6} *	−3.42	−0.15
3.007	0.119	0.0478	0.0987	6.55×10^{-6} *	−3.64	0.15

* calculated values; ** Δlog *m* Au = log *m* Au(calc.) − log *m* Au(exp.).

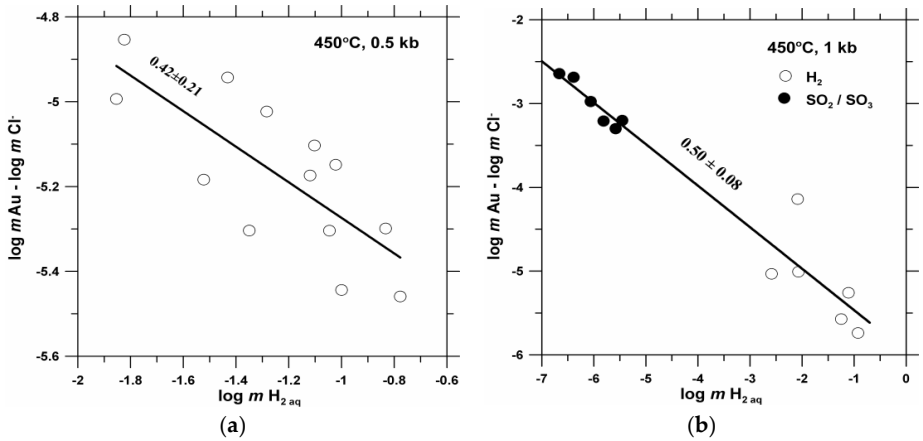

Figure 2. *Cont.*

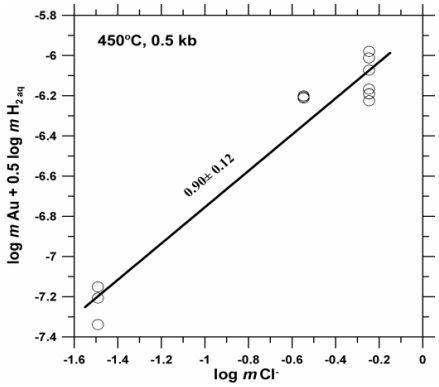

(**c**)

Figure 2. (**a**) The concentration of Au (corrected for Cl^- concentration according to Equation (2)) as a function of $H_2{}^\circ_{(aq)}$ concentration under reduced conditions. (**b**) The concentration of Au (corrected for Cl^- concentration) as a function of $H_2{}^\circ_{(aq)}$ concentration under reduced to oxidized conditions. (**c**) The concentration of Au (corrected for the of $H_2{}^\circ_{(aq)}$ concentration) as a function of Cl^- concentration under reduced conditions.

The differences between the experimental and calculated Au solubility values (last two columns of Table 1) do not exceed 0.2 log units and are independent of NaCl concentration in the wide range of fluid salinities (from 0.1 to 3 mol·(kg·H_2O)$^{-1}$), HCl concentrations, and redox conditions (Figure 3). This confirms the high accuracy of our method of the calculation of activity coefficients (in particular, the constant value of the ion size parameter $\overset{o}{a}$ = 4.5 Å), including the activity coefficient of $H_2{}^\circ_{(aq)}$, which was calculated ignoring the salting-out effect even in concentrated NaCl solutions.

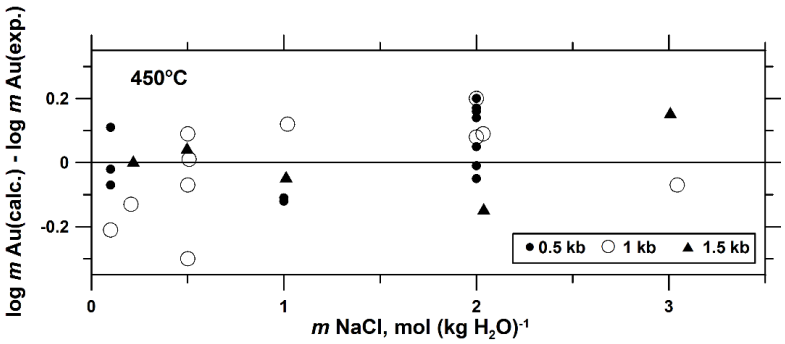

Figure 3. Difference between Au solubilities calculated using Equation (5) and observed in the experiments vs. NaCl molality.

3.2. Au Solubility Constant at 25–1000 °C and Pressures up to 5 kbar

The Au solubility constant values, log $K_s{}^\circ$, determined in this study are given in Table 2 together with values obtained from the literature data. The log $K_s{}^\circ$ values are plotted as a function of temperature and pressure in Figure 4. Nikolaeva et al. [3] determined the electromotive force (e.m.f.) of the reaction

$$AuCl_2{}^- + 0.5H_{2(g)} = Au + 2Cl^- + H^+ \quad (4)$$

at 25–80 °C and saturated vapor pressure ($P_{sat.}$). The ionic strength of experimental solutions was fixed at 1 M. In the present study, the data of [3] were corrected for ionic strength for the calculation of the thermodynamic value of Au solubility constant (Supplementary Material Section 2). Experimental Au solubility data reported by Ryabchikov and Orlova [7] (750 °C, 1500 bar, Supplementary Material Section 3.1), Guo et al. [9] (800 °C, 2000 bar, Supplementary Material Section 3.2), and Zajacz et al. [8]

(1000 °C, 1500 bar, Supplementary Material Section 3.3) were evaluated using the OptimA computer code for the calculation of log $K_s°$. The results of regression analysis are summarized in the Supplementary Materials together with the original experimental data. In the calculation we used the experimental data of Guo et al. [9] obtained under redox conditions reliably controlled by the Ni-NiO, Fe_3O_4-Fe_2O_3, MnO-Mn_3O_4 buffers (five experiments in total). Experimental data of Zajacz et al. [8] for sulfur-free NaCl-HCl-H_2 fluids were used in our calculations, because thermodynamic data for sulfur-bearing species are highly uncertain at the experimental *T*-*P* parameters. The Au solubility constant reported by Gammons and Willams-Jones [4] for 300 °C and $P_{sat.}$ was recalculated to satisfy Equation (3) as described in Supplementary Material Section 3.4.

The Au solubility constants obtained in the present study and values calculated from the literature data were fitted to a simple density model (Anderson et al. [28]),

$$\log K_s° = 4.302 - 7304 \cdot T(\mathrm{K})^{-1} - 4.77 \cdot \log d(\mathrm{w}) + 11080 \cdot (\log d(\mathrm{w})) \cdot T(\mathrm{K})^{-1} - 6.94 \times 10^6 \cdot (\log d(\mathrm{w})) \cdot T(\mathrm{K})^{-2} \quad (5)$$

where d(w) is the pure water density. The calculated values of log $K_s°$ are listed in Table 3, compared with the experimental data in Figure 4, and with the literature theoretical models in Figures S1 and S2 of the Supplementary Materials. The values of Gibbs free energy of $AuCl_2^-$, calculated using Equation (5), are tabulated in Table S14 of the Supplementary Materials. The values of Gibbs free energy of aqueous species—components of the experimental systems, for which we used equations of state other than HKF (Helgeson, Kirkham, Flowers) are listed in Table S15 (NaCl°), Table S16 (SO_2°), Table S17 (O_2°), and Table S18 (H_2°) of the Supplementary Materials. During the fit of log $K_s°$ to the density model, the statistical weights of log $K_s°$ values were set to 2 for the 25 °C data (Nikolaeva et al. [3]) and 0.5 for $t \geq 750$ °C, because of the higher uncertainty of the thermodynamic properties of aqueous ions and electrolytes at high temperatures. The fit quality, expressed as the standard deviation of the difference between the calculated and experimental log $K_s°$ values, is equal to 0.12, which is close to the experimental uncertainty (Table 2). As can be seen in Figure 4, the dependence of log $K_s°$ on the reciprocal absolute temperature is close to linear. This supports the plausibility of the Au solubility reaction (Equation (2)), which can be considered as isocoulombic ($\Delta_r C_p°$ ~0).

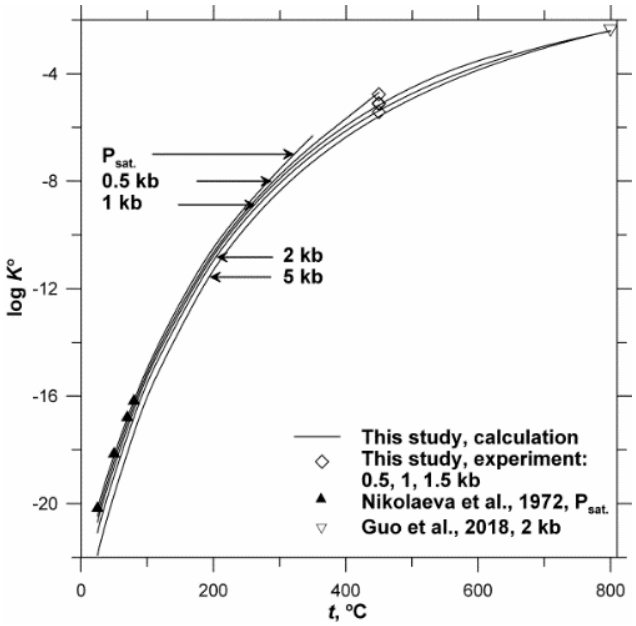

Figure 4. *Cont.*

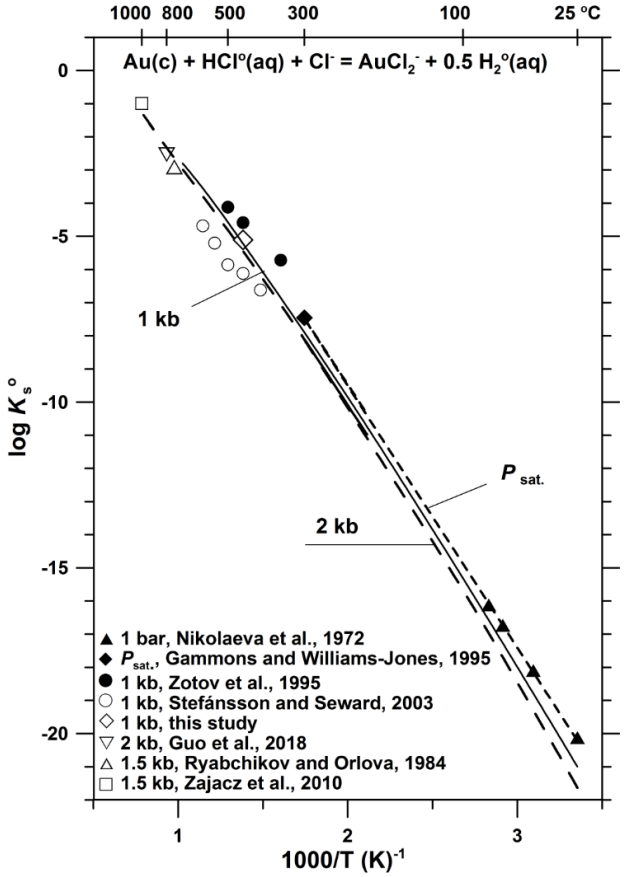

Figure 4. The Au solubility constant (Equation (3)) as a function of pressure and reciprocal temperature. Symbols are experimental data, and lines were calculated using Equation (5). The effect of pressure up to 5 kbar is shown in the insert.

Table 2. Comparison of experimental values of the Au solubility constant (Equation (3)) with model values calculated using Equation (5): $\log K_s^\circ = 4.302 - 7304 \cdot T(\mathrm{K})^{-1} - 4.77 \cdot \log d(\mathrm{w}) + 11080 \cdot (\log d(\mathrm{w})) \cdot T(\mathrm{K})^{-1} - 6.94 \times 10^6 \cdot (\log d(\mathrm{w})) \cdot T(\mathrm{K})^{-2}$, where d(w) is the pure water density.

t, °C	*P*, bar	log K_s° (exp.)	log K_s° (calc.)	Δlog K_s° (calc. − exp.)	Reference
450	500	−4.77 ± 0.07	−4.72	0.05	This study
450	1000	−5.10 ± 0.09 *	−5.22	−0.12	*Ibid.*
450	1000	−5.12 ± 0.06 **	−5.22	−0.10	*Ibid.*
450	1500	−5.43 ± 0.09	−5.36	0.07	*Ibid.*
25	1	−20.12 ± 0.08	−20.14	−0.02	Nikolaeva et al. [3]
50	1	−18.09 ± 0.08	−18.11	−0.02	*Ibid.*
70	1	−16.74 ± 0.07	−16.68	0.06	*Ibid.*
80	1	−16.12 ± 0.07	−16.02	0.10	*Ibid.*
300	$P_{sat.}$	−7.46 ± 0.40	−7.47	−0.01	Gammons and Williams-Jones [4]
750	1500	−2.91 ± 0.30	−2.59	0.32	Ryabchikov and Orlova [7]
800	2000	−2.54 ± 0.20	−2.33	0.21	Guo et al. [9]
1000	1500	−0.99 ± 0.20	−1.23	−0.24	Zajacz et al. [8]

* Au-NaCl-HCl-H_2-H_2O system; ** Au-NaCl-HCl-H_2SO_4-SO_2-H_2O system.

The experiments reported here fall within the *T*-*P* range of the key studies of Au solubility in chloride fluids performed by Zotov et al. [5] and Stefánsson and Seward [6] (Supplementary Material Section 3.5). Our Au solubility data are 0.5 log units lower than those of [5]. At 350 °C the difference between the log K_s° values predicted by Equation (5) and data of [5] increases to one log unit. This disagreement can be explained by partial loss of hydrogen, whose concentration was calculated, but

not measured in [5]. In contrast, the log K_s° values reported by Stefánsson and Seward [6] are one log unit lower compared with our results. The reason for this disagreement is unclear.

Table 3. The Au solubility constant of the reaction $Au_{(cr)} + HCl^\circ_{(aq)} + Cl^- = AuCl_2^- + 0.5H_2{}^\circ_{(aq)}$ as a function of temperature and pressure. Calculations were performed using Equation (5) obtained in the present study.

t, °C	Pressure, bar					
	$P_{sat.}$	500	1000	1500	2000	5000
25	−20.14	−20.56	−20.93	−21.27	−21.57	−22.96
100	−14.83	−15.06	−15.27	−15.46	−15.63	−16.41
200	−10.33	−10.55	−10.71	−10.84	−10.95	−11.42
250	−8.79	−8.99	−9.15	−9.27	−9.37	−9.76
300	−7.47	−7.72	−7.89	−8.00	−8.09	−8.43
350	−6.25	−6.65	−6.85	−6.97	−7.05	−7.34
400		−5.69	−5.97	−6.10	−6.18	−6.44
450		−4.72	−5.22	−5.36	−5.45	−5.68
500		−3.94	−4.58	−4.73	−4.82	−5.02
550			−4.02	−4.19	−4.27	−4.45
600			−3.56	−3.71	−3.79	−3.95
650			−3.16	−3.30	−3.37	−3.51
700			−2.81	−2.93	−2.99	−3.11
750				−2.59	−2.64	−2.76
800				−2.28	−2.33	−2.43
850				−2.00	−2.04	−2.13
900				−1.73	−1.77	−1.85
950				−1.47	−1.51	−1.60
1000				−1.23	−1.27	−1.36

4. Discussion

4.1. Effect of Temperature, pH, and Chlorinity on Au Solubility

The range of chlorinity of aqueous fluids used to derive Equation (5) extends from pure HCl to 4.4*m* NaCl (20 wt % NaCl). In our recent study (Tagirov et al. [29]), the speciation of Au was studied by means of X-ray absorption spectroscopy and ab initio molecular dynamics up to 4*m* HCl/7*m* KCl (34 wt % KCl). Moreover, the experimental spectra were acquired and theoretical calculations were performed for dry (anhydrous) chloride melts. It was demonstrated that at high temperatures the microscopic state (local atomic environments) of the system is identical over the whole range of chloride concentrations, from dilute fluids to dry melts. This means that $AuCl_2^-$ is the main chloride complex at any chloride concentration at fluid density $d > 0.3$ g·cm^{-3} (this density corresponds to the experimental *T-P* parameters of the study of Zajacz et al. [8]). The study [29] and the present work clearly demonstrate that there is no need to invoke ionic associates, such as $NaAuCl_2^\circ$ and $HAuCl_2^\circ$, to describe Au solubility. The solubility of Au in high temperature fluids and brines can be accurately calculated, as described in Section 2.2, using the equilibrium constant of reaction (2) and the extended Debye–Hückel equation for the activity coefficients of aqueous species (Equation (1)). At lower densities ($d < 0.3$ g·cm^{-3}), the simple neutral complex $AuCl^\circ_{(aq)}$ predominates Au speciation (Archibald et al. [12]).

The excellent agreement between Au solubilities calculated by Equation (5) and experimental data in the wide range of *T-P* parameters (from 25 to 1000 °C and from $P_{sat.}$ to 2000 bar) enables accurate prediction of Au mobilization in most natural environments where ore metals are transported and deposited by chloride-rich fluids. The effect of temperature, pH, and fluid salinity on Au solubility is shown in Figure 5. This diagram was constructed for a redox state buffered by the Ni–NiO equilibrium and salinities of (i) 1*m* NaCl, which is typical, for example, of relatively low-temperature (300–400 °C) seafloor hydrothermal systems (Bortnikov et al. [30]; Hannington et al. [31]) and

high-temperature magmatic fluids (800 °C) separated from arc dacite magma of porphyry-generating intrusion (Blundy et al. [32]); and (ii) 7*m* NaCl which is typical of magmatic brine inclusions and products of the separation of single-phase magmatic fluids (Seward et al. [1], Aranovich et al. [33]). At a low temperature of 200 °C, hydrosulfide complexes predominate at any pH and chlorinity (Seward et al. [1], Trigub et al. [34]). The maximum solubility is observed in near-neutral solutions in the $Au(HS)_2^-$ predominance region with pH ~pK_{H2S} (that is, at similar concentrations of $H_2S^\circ_{(aq)}$ and HS^-, which are necessary for the formation of the Au complex). As temperature increases, the Au concentration of acidic solution starts to increase, because the Au solubility is controlled in this region by $AuCl_2^-$ (Equation (2)). In the $AuCl_2^-$ predominance region, the Au solubility increases systematically with increasing temperature and fluid acidity. The Au concentration in 7*m* NaCl at neutral pH can reach a few hundred ppb at 500 °C and 1 kbar and increases by three orders of magnitude at 800 °C and 2 kbar. We note that the Au concentration at the minima of the solubility curves is weakly dependent on *T, P,* and fluid chemistry and is close to 10 ppb at the given redox state (Ni-NiO) and H_2S molality (0.01*m*). In this region, $AuHS^\circ_{(aq)}$ dominates at $t \leq 400$ °C, and $Au(OH)^\circ_{(aq)}$ becomes the main Au complex at higher temperatures.

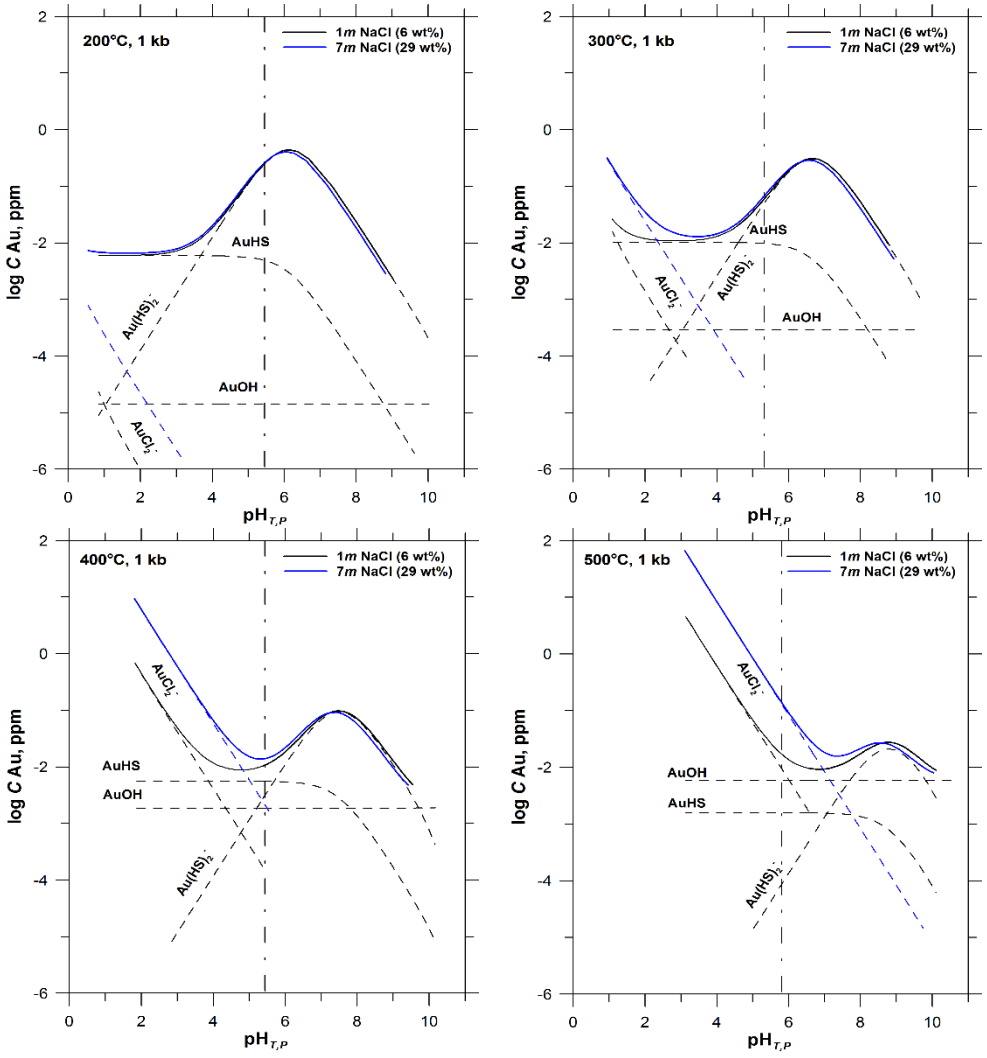

Figure 5. *Cont.*

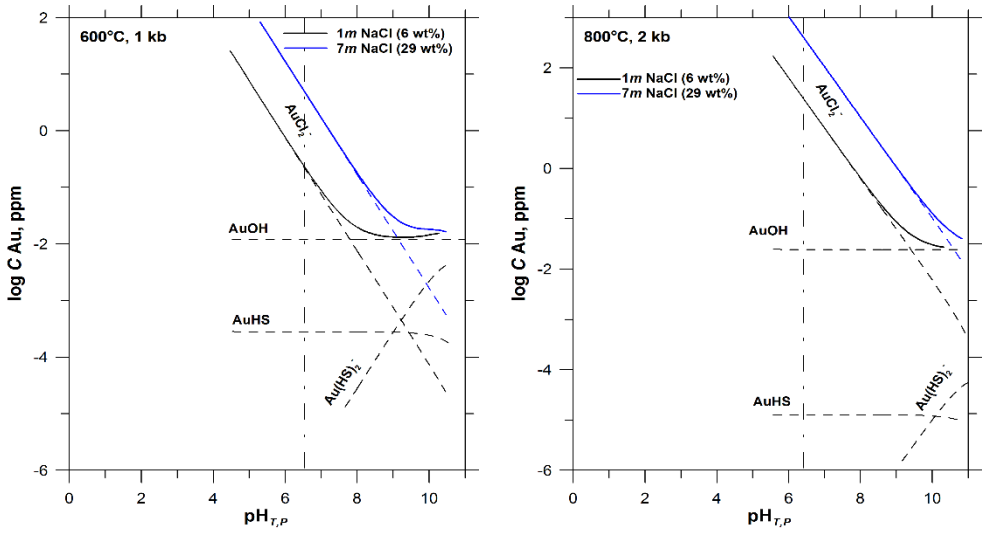

Figure 5. Gold solubility as a function of $pH_{T,P}$. The concentration of dissolved sulfur is 0.01 m, the redox conditions are controlled by the Ni/NiO buffer. Lines are calculated using the results of the present study: solid lines—total dissolved Au, and dashed lines—individual aqueous complexes. The vertical dashed-dotted line corresponds to neutral pH. Thermodynamic data for Au–OH and Au–HS complexes were adopted from Akinfiev and Zotov [35].

4.2. Gold Concentration in Natural Fluids

Figure 6 compares the Au concentrations calculated using Equation (5) with the data of Ulrich et al. [2] for high-temperature fluid inclusions of the Bajo de la Alumbrera porphyry Cu–Au deposit (Argentina). The highest-temperature primary brine inclusions from this deposit (650–770 °C, 50–60 wt % NaCl eq.) contain 0.55 ppm Au. The hydrothermal fluids of porphyry systems are usually oxidized, and the redox state can be considered close to the hematite-magnetite buffer. The calculated Au solubility in the chloride brine of the Bajo de la Alumbrera deposit is ~10^3 times higher than the measured Au concentration (0.55 ppm). This implies that the high-temperature ore fluids are strongly undersaturated with respect to native Au. Therefore, at high temperatures during the early stages of porphyry ore formation, Au can be deposited only in an "invisible" (or refractory) state, either in the form of nanoscale particles or as a component of solid solutions (e.g., Tagirov et al. [36], Trigub et al. [37]). A decrease in temperature results in a drastic decrease in Au solubility. The Au saturation limit of 0.55 ppm is attained at a temperature of slightly above 400 °C at 1 kbar under the hematite-magnetite buffer redox conditions. At these conditions, the deposition of native gold becomes possible, which is consistent with estimates for ore precipitation at the Bajo de la Alumbrera deposit.

Figure 7 shows Au solubility as a function of fluid chlorinity at temperatures from 300 to 1000 °C. The pH values are controlled by silicate mineral buffers, and the redox state, by the hematite–magnetite buffer. At the given KCl concentration, the pH values range from near-neutral to weakly acidic. Another feature of fluid systems buffered by mineral assemblages is that the muscovite–andalusite–quartz buffer yields more acidic pH values (black lines in Figure 7) than the K-feldspar–muscovite–quartz buffer (blue lines). At subcritical temperatures and near-neutral pH values imposed by fluid interaction with silicate mineral assemblages, the hydroxide complex $AuOH^\circ$ dominates over the whole range of chlorinity up to 60 wt % NaCl eq. An increase in temperature results in an increase in dissolved Au concentration. At low Cl concentrations in the $AuOH^\circ$ predominance region, an increase in temperature from 400 to 1000 °C results in an increase in Au solubility from 10 to 400 ppb. At higher chlorinities in the $AuCl_2^-$ predominance region, an increase in Cl concentration results in an increase in Au solubility, which can reach at 10 wt % NaCl eq. ~1 ppm at 500 °C and ~1000 ppm at 1000 °C. We note again that the pH values are near-neutral at both temperatures: pH ~5.3 at 500 °C/1 kbar and ~8 at 1000 °C/2 kbar (neutral pH is 5.8 and 7.4, respectively). Therefore,

despite the neutral pH conditions, the Au solubility in high-temperature fluids is sufficiently high, owing to the high stability of $AuCl_2^-$, for efficient Au transport even in Au-undersaturated fluids.

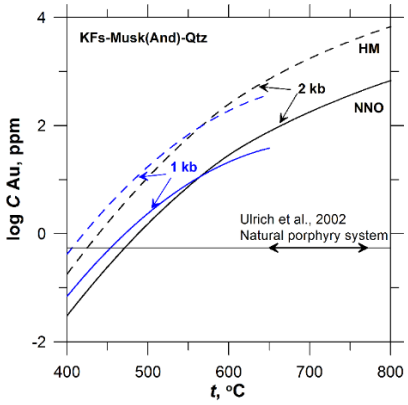

Figure 6. The solubility of Au as a function of temperature at 1 and 2 kbar (blue and black lines, respectively). The pH value is controlled by the K-feldspar–muscovite–quartz buffer at t < 550 °C at 1 kbar and t < 600 °C at 2 kbar and the K-feldspar–andalusite–quartz buffer at higher temperatures. The redox state of the system corresponds to the Fe_2O_3/Fe_3O_4 (HM) and Ni/NiO (NNO) buffers. The horizontal line shows the concentration of Au (0.55 ppm) determined in the highest-temperature fluid inclusions from the Bajo de la Alumbrera porphyry Cu–Au deposit (Argentina, Ulrich et al. [2]).

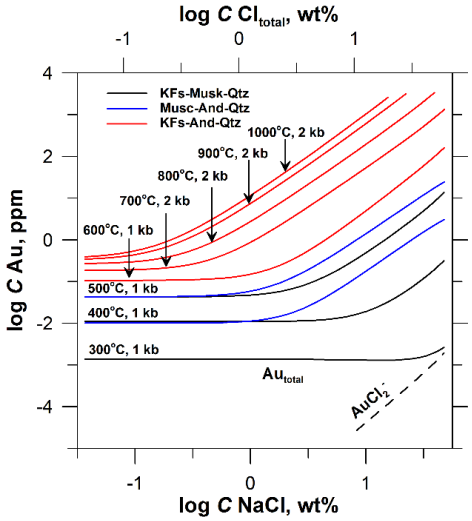

Figure 7. The solubility of Au as a function of fluid chlorinity for S-free system. The concentration of KCl is fixed as m(KCl) = 1/5 m(NaCl). The pH value is controlled by the K-feldspar–muscovite–quartz, muscovite–andalusite–quartz, and K-feldspar–andalusite–quartz buffers. Horizontal segments of the solubility curves correspond to the AuOH° predominance fields. Thermodynamic data for Au–OH complexes are adopted from Akinfiev and Zotov [35].

5. Conclusions

The solubility of Au was measured at 450 °C and pressures of 500, 1000, and 1500 bar in a wide range of fluid chlorinity, from 0.1m to 3m NaCl. The redox state of the experimental system was controlled either by hydrogen added to the autoclave (reduced conditions), or by the SO_2/SO_3 buffer (oxidized conditions). The measured Au solubilities are best described by the formation of the $AuCl_2^-$ complex. The equilibrium Au solubility constants calculated for the contrasting redox states are in perfect agreement with each other and fall between the values reported by Zotov et al. [5] and

Stefánsson and Seward [6]. The experimental values of the Au solubility constant were fitted together with Au solubility data available in the literature for temperatures from 25 to 1000 °C and pressures up to 2 kbar to a simple density model equation. The equation describes the experimental data with an accuracy approaching the experimental uncertainties in the whole region of *T*-*P* parameters and can be used to predict Au solubility at pressures up to 5 kbar. The results of our study demonstrate that the simple complex $AuCl_2^-$ predominates Au speciation in natural fluids in a wide range of salinity at fluid densities $d > 0.3$ g·cm^{-3}. The solubility of Au can be accurately calculated at solute concentrations up to at least 5*m* NaCl eq. using the equilibrium constant of the reaction of $AuCl_2^-$ formation and the extended Debye–Hückel equation for activity coefficients. Thermodynamic calculations performed using the obtained results showed that the formation of $AuCl_2^-$ can account for efficient hydrothermal transport of Au at $t > 400$ °C and any chlorinity of hydrothermal fluid whose density (d) is > 0.3 g·cm^{-3}. At $t < 400$ °C hydroxide and hydrosulfide complexes become the dominant Au species. At $d < 0.3$ g·cm^{-3} the role of $AuCl_2^-$ is masked by the formation of $AuCl^\circ$.

Supplementary Materials: The following are available online at http://www.mdpi.com/2075-163X/8/7/286/s1, Table S1: The log K° values of the reaction $Na^+ + Cl^- = NaCl^\circ_{(aq)}$, Table S2: The log K° values of the reaction $HCl^\circ_{(aq)} = H^+ + Cl^-$, Table S3: The log K° values of the reaction $H_{2(g)} = H_2{}^\circ_{(aq)}$, Table S4: The log K° values of the reaction $O_{2(g)} = O_2{}^\circ_{(aq)}$, Table S5: The log K° values of the reaction $SO_{2(g)} = SO_2{}^\circ_{(aq)}$, Table S6: The log K° values of the reaction $H_2O_{(l)} = H^+ + OH^-$, Table S7: Calculation of Gibbs free energy of $AuCl_2^-$ using data of Nikolaeva et al., Table S8: Calculation of equilibrium constant of Au solubility reaction using data of Nikolaeva et al., Table S9: Treatment of experimental data of Ryabchikov and Orlova, Table S10: Treatment of experimental data of Guo et al., Table S11: Treatment of experimental data of Zajacz et al., Table S12: Recalculation of data of Gammons and Williams-Jones into the Au solubility constant, Table S13: Original and recalculated values of Au solubility constant, log $K_s{}^\circ$, based on data of Zotov et al. and Stefánsson and Seward, Table S14: Gibbs free energy of $AuCl_2^-$, Table S15: Gibbs free energy of $NaCl^\circ_{(aq)}$, Table S16: Gibbs free energy of $SO_2{}^\circ_{(aq)}$, Table S17: Gibbs free energy of $O_2{}^\circ_{(aq)}$, Table S18: Gibbs free energy of $H_2{}^\circ_{(aq)}$.

Author Contributions: A.V.Z. and B.R.T. designed and performed the experiments and thermodynamic calculations, and wrote the paper; N.N.K. participated in the experimental work and data treatment; V.L.R. performed technical operations and participated in the experimental work; all the authors participated in the manuscript preparation.

Funding: This study was supported by the Russian Science Foundation, grant No. 17-17-01220 (experimental work and data treatment) and the Base Theme of IGEM RAS (compilation of literature data).

Acknowledgments: We thank Dmitry Petrenko for determination of Au concentrations and Ludmila Koroleva for determination of SO_2 concentrations. Nikolai Akinfiev is acknowledged for useful discussions during the manuscript preparation. We are grateful to Andrey Girnis for English grammar correction. The authors thank three anonymous reviewers and Galina Palyanova for helpful comments and suggestions. Chemical analyses were carried out at the "IGEM-Analytica" Center for collective use.

Conflicts of Interest: The authors declare no conflict of interest.

References

1. Seward, T.M.; Williams-Jones, A.E.; Migdisov, A.A. The chemistry of metal transport and deposition by ore-forming hydrothermal fluids. In *Treatise on Geochemistry*, 2nd ed.; Turekian, K., Holland, H., Eds.; Elsevier: New York, NY, USA, 2014; Volume 13, pp. 29–57.
2. Ulrich, T.; Günther, D.; Heinrich, C.A. The Evolution of a porphyry Cu-Au deposit, based on LA-ICP-MS analysis of fluid inclusions: Bajo de la Alumbrera, Argentina. *Econ. Geol.* **2001**, *96*, 1743–1774. [CrossRef]
3. Nikolaeva, N.M.; Erenburg, A.M.; Antipina, V.A. About the temperature dependence of standard potentials of halide complexes of gold. *Izvestiya Sibirskogo Otdeleniya Akademii Nauk SSSR Seriya Khimicheskih Nauk* **1972**, *4*, 126–128. (In Russian)
4. Gammons, C.H.; Williams-Jones, A.E. The solubility of Au-Ag alloy + AgCl in HCl/NaCl solutions at 300 °C: New data on the stability of Au(I) chloride complexes in hydrothermal fluids. *Geochim. Cosmochim. Acta* **1995**, *59*, 3453–3468. [CrossRef]

5. Zotov, A.V.; Kudrin, A.V.; Levin, K.A.; Shikina, N.D.; Var'yash, L.N. Experimental studies of the solubility and complexing of selected ore elements (Au, Ag, Cu, Mo, As, Sb, Hg) in aqueous solutions. In *Fluids in the Crust. Equilibrium and Transport Properties*; Shmulovich, K.I., Yardley, B.W.D., Gonchar, G.G., Eds.; Springer: Dordrecht, The Netherlands, 1995; pp. 95–137.
6. Stefánsson, A.; Seward, T.M. Stability of chloridogold(I) complexes in aqueous solutions from 300 to 600 °C and from 500 to 1800 bar. *Geochim. Cosmochim. Acta* **2003**, *67*, 4559–4576. [CrossRef]
7. Ryabchikov, I.D.; Orlova, G.P. Gold in magmatic fluids. In *Phizico-khimicheskie Modeli Petrogeneza i Rudoobrazovaniya*; Nauka Press: Novosibirsk, Russia, 1984; pp. 103–111. (In Russian)
8. Zajacz, Z.; Seo, J.H.; Candela, P.A.; Piccoli, P.M.; Heinrich, C.A.; Guillong, M. Alkali metals control the release of gold from volatile-rich magmas. *Earth Planet. Sci. Lett.* **2010**, *297*, 50–56. [CrossRef]
9. Guo, H.; Audétat, A.; Dolejš, D. Solubility of gold in oxidized, sulfur-bearing fluids at 500–850 °C and 200–230 MPa: A synthetic fluid inclusion study. *Geochim. Cosmochim. Acta* **2018**, *222*, 655–670. [CrossRef]
10. Pokrovski, G.S.; Tagirov, B.R.; Schott, J.; Bazarkina, E.F.; Hazemann, J.-L.; Proux, O. An in situ X-ray absorption spectroscopy study of gold-chloride complexing in hydrothermal fluids. *Chem. Geol.* **2009**, *259*, 17–29. [CrossRef]
11. Mei, Y.; Liu, W.; Sherman, D.M.; Brugger, J. Metal complexing and ion hydration in low density hydrothermal fluids: Ab initio molecular dynamics simulation of Cu(I) and Au(I) in chloride solutions (25–1000 °C, 1–5000 bar). *Geochim. Cosmochim. Acta* **2014**, *131*, 196–212. [CrossRef]
12. Archibald, S.M.; Migdisov, A.A.; Williams-Jones, A.E. The stability of Au-chloride complexes in water vapor at elevated temperatures and pressures. *Geochim. Cosmochim. Acta* **2001**, *65*, 4413–4423. [CrossRef]
13. Kudrin, A.V. Behaviour of Mo in aqueous NaCl and KCl solutions at 300–450 °C. *Geochem. Int.* **1989**, *26*, 87–99.
14. Driesner, T. The system H_2O-NaCl. II. Correlations for molar volume, enthalpy, and isobaric heat capacity from 0 to 1000 °C, 1 to 5000 bar, and 0 to 1 X_{NaCl}. *Geochim. Cosmochim. Acta* **2007**, *71*, 4902–4919. [CrossRef]
15. Driesner, T.; Heinrich, C.A. The system H_2O-NaCl. I. Correlation formulae for phase relations in temperature-pressure-composition space from 0 to 1000 °C, 0 to 5000 bar, and 0 to 1 X_{NaCl}. *Geochim. Cosmochim. Acta* **2007**, *71*, 4880–4901. [CrossRef]
16. Zotov, A.V.; Baranova, N.N. Thermodynamic properties of the aurochloride solute complex $AuCl_2^-$ at temperatures of 350–500 °C and pressures of 500–1500 bars. *Sciences Géologiques Bulletins Mémoires* **1989**, *42*, 335–342. [CrossRef]
17. Shvarov, Y.V. HCh: New potentialities for the thermodynamic simulation of geochemical systems offered by Windows. *Geochem. Int.* **2008**, *46*, 834–839. [CrossRef]
18. Johnson, J.W.; Oelkers, E.H.; Helgeson, H.C. SUPCRT92: A software package for calculating the standard molal thermodynamic properties of minerals, gases, aqueous species, and reactions from 1 to 5000 bar and 0 to 1000 °C. *Comput. Geosci.* **1992**, *18*, 899–947. [CrossRef]
19. Wagner, W.; Pruss, A. The IAPWS formulation 1995 for the thermodynamic properties of ordinary water substance for general and scientific use. *J. Phys. Chem. Ref. Data* **2002**, *31*, 387–535. [CrossRef]
20. Tagirov, B.R.; Zotov, A.V.; Akinfiev, N.N. Experimental study of dissociation of HCl from 350 to 500 °C and from 500 to 2500 bars: Thermodynamic properties of $HCl_{(aq)}$. *Geochim. Cosmochim. Acta* **1997**, *61*, 4267–4280. [CrossRef]
21. Ho, P.C.; Palmer, D.A.; Mesmer, R.E. Electrical conductivity measurements of aqueous sodium chloride solutions to 600 °C and 300 MPa. *J. Solut. Chem.* **1994**, *23*, 997–1018. [CrossRef]
22. Bandura, A.V.; Lvov, S.N. The ionization constant of water over wide ranges of temperature and density. *J Phys. Chem. Ref. Data* **2006**, *35*, 15–30. [CrossRef]
23. Akinfiev, N.N.; Diamond, L.W. Thermodynamic description of aqueous nonelectrolytes at infinite dilution over a wide range of state parameters. *Geochim. Cosmochim. Acta* **2003**, *67*, 613–627. [CrossRef]
24. Robie, R.A.; Hemingway, B.S. *Thermodynamic Properties of Minerals and Related Substances at 298.15 K and 1 bar (10^5 Pascals) Pressure and at Higher Temperatures, U.S. Geological Survey Bulletin 2131*; U.S. Government Printing Office: Washington, DC, USA, 1995.
25. Berman, R.G. Internally consistent thermodynamic data for minerals in the system Na_2O-K_2O-CaO-MgO-FeO-Fe_2O_3-Al_2O_3-SiO_2-TiO_2-H_2O-CO_2. *J. Petrol.* **1988**, *29*, 445–522. [CrossRef]
26. Sverjensky, D.A.; Hemley, J.J.; D'Angelo, M.D. Thermodynamic assessment of hydrothermal alkali feldspar-mica-aluminosilicate equilibria. *Geochim. Cosmochim. Acta* **1991**, *55*, 989–1004. [CrossRef]

27. Shvarov, Y. A suite of programs, OptimA, OptimB, OptimC, and OptimS compatible with the Unitherm database, for deriving the thermodynamic properties of aqueous species from solubility, potentiometry and spectroscopy measurements. *Appl. Geochem.* **2015**, *55*, 17–27. [CrossRef]
28. Anderson, G.M.; Castet, S.; Schott, J.; Mesmer, R.E. The density model for estimation of thermodynamic parameters of reactions at high temperatures and pressures. *Geochim. Cosmochim. Acta* **1991**, *55*, 1769–1779. [CrossRef]
29. Tagirov, B.R.; Trigub, A.L.; Filimonova, O.N.; Kvashnina, K.O.; Nickolsky, M.S.; Lafuerza, S.; Chareev, D.A. Gold speciation and solubility in chloride fluids and melts: Insights from X-ray absorption spectroscopy, Ab initio molecular dynamics and thermodynamic modeling. *Geochim. Cosmochim. Acta* **2018**. under review.
30. Bortnikov, N.S.; Simonov, V.A.; Bogdanov, Y.A. Fluid inclusions in minerals from modern sulfide edifices: Physicochemical conditions of formation and evolution of fluids. *Geol. Ore Depos.* **2004**, *46*, 64–75.
31. Hannington, M.D.; de Ronde, C.D.J.; Petersen, S. Sea-floor tectonics and submarine hydrothermal systems. In *Economic Geology 100th Anniversary Volume*; Henderquist, J.W., Thompson, J.F.H., Goldfarb, R.J., Richards, J.P., Eds.; Society of Economic Geologists: Littelton, CO, USA, 2005; pp. 111–141.
32. Blundy, J.; Mavrogenes, J.; Tattitch, B.; Sparks, S.; Gilmer, A. Generation of porphyry copper deposits by gas–brine reaction in volcanic arcs. *Nat. Geosci.* **2015**, *8*, 235–240. [CrossRef]
33. Aranovich, L.Y.; Newton, R.C.; Manning, C.E. Brine-assisted anatexis: Experimental melting in the system haplogranite–H_2O–NaCl–KCl at deep-crustal conditions. *Earth Plan. Sci. Lett.* **2013**, *374*, 111–120. [CrossRef]
34. Trigub, A.L.; Tagirov, B.R.; Kvashnina, K.O.; Lafuerza, S.; Filimonova, O.N.; Nickolsky, M.S. Experimental determination of gold speciation in sulfide-rich hydrothermal fluids under a wide range of redox conditions. *Chem. Geol.* **2017**, *471*, 52–64. [CrossRef]
35. Akinfiev, N.N.; Zotov, A.V. Thermodynamic description of aqueous species in the system Cu-Ag-Au-S-O-H at temperatures of 0–600 °C and pressures of 1–3000 bar. *Geochem. Int.* **2010**, *48*, 714–720. [CrossRef]
36. Tagirov, B.R.; Trigub, A.L.; Kvashnina, K.O.; Shiryaev, A.A.; Chareev, D.A.; Nickolsky, M.S.; Abramova, V.D.; Kovalchuk, E.V. Covellite CuS as a matrix for "invisible" gold: X-ray spectroscopic study of the chemical state of Cu and Au in synthetic minerals. *Geochim. Cosmochim. Acta* **2016**, *191*, 58–69. [CrossRef]
37. Trigub, A.L.; Tagirov, B.R.; Kvashnina, K.O.; Chareev, D.A.; Nickolsky, M.S.; Shiryaev, A.A.; Baranova, N.N.; Kovalchuk, E.V.; Mokhov, A.V. X-ray spectroscopy study of the chemical state of "invisible" Au in synthetic minerals in the Fe-As-S system. *Am. Mineral.* **2017**, *102*, 1057–1065.

© 2018 by the authors. Licensee MDPI, Basel, Switzerland. This article is an open access article distributed under the terms and conditions of the Creative Commons Attribution (CC BY) license (http://creativecommons.org/licenses/by/4.0/).